A high-resolution, 3D groundwater-surface water simulation of the contiguous US: Advances in the integrated ParFlow CONUS 2.0 modeling platform

Chen Yang[1,2], Danielle T. Tijerina-Kreuzer[1,2], Hoang V. Tran[3], Laura E. Condon[4], Reed M. Maxwell[1,2,5]

[1]Department of Civil and Environmental Engineering, Princeton University, Princeton, NJ, USA

[2]Integrated GroundWater Modeling Center, Princeton University, Princeton, NJ, USA

[3]Atmospheric Science & Global Change Division, Pacific Northwest National Laboratory, Richland, WA, USA

[4]Department of Hydrology and Atmospheric Sciences, University of Arizona, Tucson, AZ, USA

[5]High Meadows Environmental Institute, Princeton University, Princeton, NJ, USA

Corresponding to:
Chen Yang, cy15@princeton.edu
Laura Condon, lecondon@arizona.edu
Reed Maxwell, reedmaxwell@princeton.edu

Abstract

Large-scale, high-resolution hydrologic modeling is an important tool to address questions of water quantity, availability, and recharge. Continental-to-Global scale models, particularly those that include groundwater, are growing in number. However, many of these approaches simplify aspects of the system and the connections between e.g., surface water and groundwater. The ParFlow CONUS modeling platform is a large-scale, hyper-resolution, hydrologic model that relies on the integrated solution of 3D partial differential equations that describe groundwater, soil, and surface water flow. The prior version, ParFlow CONUS 1.0, was the first large-scale hydrologic model that included an explicit treatment of lateral groundwater flow for the contiguous US. Here, we present the ParFlow CONUS 2.0 integrated hydrologic model. This model extends to the coastlines and contributing basins for the contiguous United States (i.e., CONUS) and is consistent with the NOAA National Water Model. Here we document the roughly five years of technical development of this platform, present steady-state simulation results, rigorously compare these results to the prior ParFlow CONUS 1.0 simulations, and evaluate the model performance based on observations. Simulated water table depth and streamflow were evaluated using more than 635K observations from USGS monitoring wells and streamflow gauges. Our results demonstrate improvement in both groundwater and surface water simulations over the prior generation model for all USGS Hydrologic Unit Code (HUC) basins. These results also suggest that this current generation hydrologic model has good to excellent streamflow performance over the entire CONUS, with almost half of the HUC subbasins exhibiting excellent performance based on normalized root-square error (RSR). These results suggest that the current generation

model approaches good performance for water table depth over the CONUS, a metric not usually compared directly at all in large-scale studies, with good-to-excellent performance exhibited over some HUC regions.

1. Introduction

Large-scale integrated hydrologic modeling has gained increasing importance due to groundwater's crucial role in the terrestrial water and energy cycles and global socioeconomic sustainability (Fan, 2015; Scanlon et al., 2023). The Earth system is currently facing unprecedented climate change and anthropogenic activities. Without the proper representation of groundwater in Earth System Models, future predictions can be systematically biased (Clark et al., 2015; Fan et al., 2019). In the past decade, several large-scale (i.e., continental to global scale) groundwater models have been developed to further our understanding of groundwater's role in the Earth system (de Graaf et al., 2015; de Graaf et al., 2017; Fan et al., 2013; Maxwell et al., 2015; Müller Schmied et al., 2021; Naz et al., 2023; Reinecke et al., 2019; Verkaik et al., 2022). While groundwater modeling is well established, continental-scale high-resolution simulations are a much more recent development, and there remain many challenges in parameterization, computation, and evaluation.

In recent years, progress has been made through advances in relevant science and technology, improved data products and data-sharing, and enhanced community-level communication and collaboration. Isotopic studies of groundwater cycling depth have provided a theoretical basis for configuring model depth, an issue that was previously challenging for conceptualization (Condon et al., 2020b; Ferguson et al., 2023; Gleeson et al., 2016; McIntosh and Ferguson, 2021). GPU (Graphics Processing Unit) acceleration is increasingly being used in Earth System Models, including groundwater models (Hokkanen et al., 2021; Yang et al., 2022; Yang et al., 2021), removing many barriers to massively parallel computing required for large-scale, hyper-resolution hydrologic modeling (Kollet et al., 2010). Global subsurface datasets, such as GLHYMPS 2.0, have been created, which distinguish more unconsolidated sediments and provide permeabilities for shallow and deep layers (Gleeson et al., 2014; Gleeson et al., 2011; Huscroft et al., 2018), thus promoting more reasonable subsurface configuration. Additionally, two reviews discuss the challenges and opportunities in large-scale groundwater modeling (Condon et al., 2021; Gleeson et al., 2021), which have helped shape community modeling approaches.

The ParFlow (PARallel Flow) CONUS modeling platform is an integrated, continental-scale hydrologic model of the contiguous United States. It simulates three-dimensional variably saturated groundwater movement and seamlessly integrates surface water. Its hyper resolution of one kilometer is superior to most large-scale hydrologic models, e.g., 6 arcmin in de Graaf et al. (2015). Its first version, the ParFlow CONUS 1.0 model (shortened to *CONUS1* hereafter), covers the majority of the continental US (~ 6.3 M km^2) (Maxwell et al., 2015). The performance of *CONUS1* has been evaluated through in-situ measurements and remote sensing products, as well as intercomparisons with other national models (O'Neill et al., 2021; Tijerina et al., 2021; Tran et al., 2022). The *CONUS1* model was the basis for follow-on studies that explored multi-scale interactions between groundwater and surface water and other related water and energy components (Condon et al., 2020a; Condon and Maxwell, 2019b; Maxwell and Condon, 2016; Maxwell et al., 2016).

Like the evolution of any modeling platform, the *CONUS1* model also has many limitations (O'Neill et al. 2021). Here we present the development of the next-generation ParFlow CONUS 2.0 model (hereafter *CONUS2*). Unlike the *CONUS1* model, which has a rectangular box domain, the *CONUS2* model covers the entire contiguous US as well as those areas in Mexico and Canada that drain into the US. In addition to expanding the model domain, we improved upon almost every model input. Some key advances are (1) improved surface water drainage, including spatially variable surface roughness, and (2) enhanced hydrostratigraphy, including expanded vertical layering and thicker subsurface representation (Tijerina-Kreuzer et al., 2023). Here we document the major features of the *CONUS2* model and discuss the long-term steady-state spinup process. We then compare the model performance with that of *CONUS1* using a large number of stream gauges and groundwater wells.

2. Model development and methods

In this section, we introduce the construction of the *CONUS2* modeling platform, including the following four parts: (1) the detailed configuration of *CONUS2* model and the major differences from *CONUS1* model, (2) a brief introduction of ParFlow simulation platform used to solve the *CONUS2* model, (3) simulations based on *CONUS2* model to achieve a steady-state representation of the integrated groundwater-surface water system, and (4) model evaluation by comparing simulated water table depth and streamflow with multi-source observation datasets.

2.1 *CONUS2* configuration and differences from *CONUS1*

The *CONUS2* model extends beyond the 6.3M km^2 original *CONUS1* domain both laterally and vertically. In Figure 1f, the *CONUS1* domain is shown as the dashed line box, while *CONUS2* is shown as the solid line box. The *CONUS2* domain covers the entire contiguous US and portions of Canada and Mexico that drain to the contiguous US. The total extent of the *CONUS2* model is 4,442 km by 3,256 km in *x* (east-west) and *y* (south-north) directions, respectively, with a horizontal resolution of 1 km. The *CONUS2* domain is comprised of active and inactive grid cells and has a total active area of 7.85 M km^2, shown as the colored areas in Figure 1 maps. The model depth is 392 m and consists of 10 layers with variable thicknesses of 200, 100, 50, 25, 10, 5, 1, 0.6, 0.3, and 0.1 m from bottom to top. A terrain-following grid (Maxwell, 2013) is adopted, generating a total of 78.5 M computing cells (7.85 M active lateral cells × 10 subsurface layers).

More than just extending the model domain, nearly all the major inputs to *CONUS2* have had significant development since *CONUS1*. CONUS1 elevations were based on the SHuttle Elevation Derivatives at multiple Scales (HydroSHEDS) digital elevation model (DEM), whereas CONUS2 elevations used the DEM of the NOAA National Water Model as a starting point. While *CONUS1* used GRASS GIS packages for topographic processing, *CONUS2* used the PriorityFlow package (Condon and Maxwell, 2019a), which was built specifically for large-scale hydrologic models. Using this tool, we developed and tested a new hydrologically consistent national topography dataset at 1 km resolution (Figure 1d). This process and the final dataset are described by Zhang et al. (2021).

We developed a spatially variable surface roughness (i.e., Manning's *n* coefficient) dataset for *CONUS2* based on land cover types, whereas the roughness of *CONUS1* varies only in stream channels as a function of the slope (Maxwell et al., 2015). *CONUS2* values of the surface roughness for streams and most land cover types were adapted from that of the National Water Model (Gochis et al., 2015), and values for land cover types not included in the National Water Model were collected from a prior roughness sensitivity study using ParFlow (Foster and Maxwell, 2019). Regarding the land cover types, the 2015 North American Land Cover 30-meter dataset (CCRS/CCMEO/NRCan et al., 2020) were mapped to the *CONUS2* grid and transformed from the FAO/UN classification system (Food and Agriculture Organization of the United Nations) to the IGBP (the International Geosphere-Biosphere Programme) classification system.

We adopted a similar approach to *CONUS1* for soil representation in *CONUS2*. Soil properties are applied to the top two meters (top four model layers) of the domain. Consistent with *CONUS1*, we used soil texture information from the soil survey geographic database (SSURGO) inside the US. For the newly expanded area outside the US, we used the gridded Global Soil Dataset for use in Earth System Models (GSDE) (Dai et al., 2019a; Dai et al., 2019b; Shangguan et al., 2014). The top 1 m (top three layers) and the bottom 1 m have different soil textures, shown in Figures 1a–b. Soil properties (e.g., saturated hydraulic conductivity K_{sat}, and the parameters of the van Genuchten model) for each soil texture are consistent with the *CONUS1* parameterization (Maxwell et al., 2015; Schaap and Leij, 1998), which are listed in the supporting information (Table S1).

Significant work was completed to improve the representation of hydrostratigraphy (i.e., the geologic properties below the soil) in *CONUS2*. *CONUS1* has a single, vertically homogeneous 100 m layer below the four soil layers. In *CONUS2*, we have six layers that extend 390 m below the four soil layers (Tijerina-Kreuzer et al., 2023). To parameterize the subsurface, we first constructed the hydrogeologic structure using two datasets: (1) GLHYMPS 1.0 dataset (Gleeson et al., 2014) to map the different hydrogeologic units (Figure 1c) and (2) dataset from Shangguan et al. (2017) to map the bedrock depth

(Figure 1e). This definition of bedrock has multiple hydrostratigraphic definitions, e.g., a confining layer, a depth to fractured bedrock, or an interface between surficial and bedrock aquifers, and is not coincident with the model bottom or a true “no flow” bedrock depth. Thus, we treat this bedrock depth as a flow barrier reducing the vertical flux across the target layer-interface by a factor of 0.001. This allows us to distinguish the upper unconfined and lower confined aquifers (Tijerina-Kreuzer et al., 2023).

For each hydrogeologic unit mapped in Figure 1c, we require a set of parameters such as hydraulic conductivity, porosity, and van Genuchten parameters. We started from the parameter values derived for *CONUS1* (Maxwell et al., 2015), but we conducted extensive tests to explore parameter adjustments as described in the next paragraph and documented in detail in Tijerina-Kreuzer et al. (2023) and Swilley et al. (2023). We applied anisotropy to all geologic units excluding the coarse-grained unconsolidated sediments and the Karst systems, allowing us to capture preferential flow caused by stratification. We reduced the vertical hydraulic conductivity of these selected geologic units using a tensor value of 0.1 in the vertical direction. We also applied *e*-folding adjustments on the indicators of geologic type at different layers by a factor varying with depth to decrease hydraulic conductivity with depth and slope.

Our model is too large to calibrate directly at the national scale, but we completed rigorous subsurface tests of hundreds of parameterizations, as documented by Tijerina-Kreuzer et al. (2023) and Swilley et al. (2023). Complete details of the subsurface development are provided in those two studies and are briefly summarized here. Tests were primarily conducted over two large-scale domains: the Upper Colorado River Basin of 280,000 km^2 and the Delaware-Susquehanna Basin of 103,000 km^2, representing distinct geologic (volcanic and sedimentary), topographic (rolling and flat) and climatic (dry-snow and wet-rain) characteristics. A broad range of model configurations were tested, including (1) different distributions of geologic unit or hydraulic conductivity value, (2) the existence or absence of flow barriers, (3) vertical anisotropy or isotropy of certain geologic units, (4) single *e*-folding of the total 390 m or multiple *e*-folding at different layers, (5) constant or variable depths of flow barriers, and (6) model depth of 392 or 1192 m.

Potential recharge (Figure 2) was applied as a forcing across the top layer of *CONUS2* to achieve a steady-state model configuration. Potential recharge was assembled as the multi-year (1950–2000) averaged daily precipitation minus multi-year averaged daily evapotranspiration (P-ET). Precipitation and ET datasets were developed by Livneh et al. (2015) with a roughly 6 km (1/16°) resolution, whereas that used in *CONUS1* has ~ 12 km (1/8°) resolution (Maurer et al., 2002). P-ET of *CONUS2* is slightly smaller than *CONUS1* in the eastern *CONUS1* domain, especially in the lower right corner of *CONUS1* (Figure 2). We obtained a P-ET ratio of *CONUS1* to *CONUS2* over the *CONUS1* domain as 1.22.

2.2 ParFlow simulation platform

Our simulations were conducted using the integrated groundwater and surface water model ParFlow v3 (Ashby and Falgout, 1996; Jones and Woodward, 2000; Kollet and Maxwell, 2006). ParFlow is an open-source model that is available on GitHub (ParFlow developers, 2022) and includes Python tools for pre/post-processing and GPU accelerator (Hokkanen et al., 2021). ParFlow solves for three-dimensional variably saturated subsurface flow using Richards' equation (Richards, 1931) and fully integrated overland flow using the kinematic wave approximated shallow water equation (Chow et al., 1988). The governing equations are omitted here since they have been described in detail in previous studies, e.g., (Kollet and Maxwell, 2006; Maxwell, 2013; Maxwell and Condon, 2016; Maxwell et al., 2015).

ParFlow employs the Newton-Krylov approach to solve the nonlinear system discretized using an implicit backward Euler differencing scheme. These solution steps achieve mass-conservation between the surface and subsurface systems of equations and give rise to the so-called integrated nature of the solution, as described in Maxwell et al. (2014). In each time step, the inexact Newton linearization is first applied, and then the resulting Jacobian system is solved by an iterative Krylov method in each Newton iteration (Jones and Woodward, 2001; Kollet and Maxwell, 2006; Maxwell, 2013). An effective multigrid preconditioner preconditioning the Jacobian system is performed to speed the convergence of the Krylov solver (Osei-Kuffuor et al., 2014). We used a linear tolerance of 10^{-10} and a nonlinear tolerance of 10^{-5} in this study to ensure convergence. ParFlow has been parallelized on the distributed platform with parallel efficiency to more than 1.6 $\times 10^4$ CPU cores on the single CPU platform and 1024 GPUs on the hybrid CPU-GPU platform (Hokkanen et al., 2021; Kollet et al., 2010).

2.3 Model simulations

We ran the CONUS2 model using the constant recharge forcing as source terms in the top layer until the model achieved a quasi-steady state. We started from a constant water table depth of 20 m in the entire domain. No-flow boundary conditions were applied to all facies of the model except the top face, which is spinup phase dependent. Our simulations were completed in two spinup phases. In the first spinup phase, a seepage face boundary condition (that removed any ponded surface water) was imposed at the top face until the total storage change was less than 6% of the potential recharge. Application of the seepage face boundary condition allows the subsurface system to equilibrate independently of streamflow. In the second spinup phase, the top boundary condition was changed to free-surface overland flow, which implements the surface water equations over any cells at the ground surface with ponded water (Kollet and Maxwell, 2006). This step is more computationally intensive but is important as it allows for the river network to form and for the groundwater and surface water systems to achieve equilibrium together. The second spinup phase was finished when the total storage change was less than 1% of the potential recharge. Overall, the two spinup phases required more than 120,000 years of simulation to achieve the final steady-state solution presented in Section 3. The first spinup phase was run on GPUs, and the second was run on CPUs. Phase one was performed on four NVIDIA A100 80-GB GPUs on the Della-GPU cluster at Princeton University. Phase two was performed on the Cheyenne supercomputer at National Center for Atmospheric Research (NCAR) using 4,096 2.3-GHz Intel Xeon E5-2697V4 cores (Computational and Information Systems Laboratory, 2019).

2.4 Model evaluation

Model performance is evaluated with respect to long-term average water table depth (WTD) and streamflow. We compared simulation results with four different datasets, two for WTD and two for streamflow (Figure 3).

- **USGS Water Table Depth (Figure 3a):** We collected daily WTD observations using the USGS Daily Values Service (https://waterservices.usgs.gov/), which were automatically recorded. We also collected historical, manually recorded USGS WTDs. We limited our analysis to data between 1950 and 2000 to maintain consistency with the time interval of potential recharge. We removed missing values (i.e., NAN) and values larger than 300 m or smaller than 0 m. Then we excluded wells with fewer than ten observations to roughly ensure the long-term variations. After filtering, we calculated long-term average WTDs from 83,471 wells located in *CONUS2*. For the comparison between *CONUS1* and *CONUS2,* wells within the *CONUS1* domain with average WTDs deeper than 100 m were excluded, which resulted in 50,923 wells for comparison. The filtering of WTDs larger than 100 m or 300 m was conducted due to the limited depths of CONUS models.

- **Fan et al. Water Table Depth (Figure 3c):** Fan et al. (2007) assembled a dataset including the average WTDs of USGS daily observations during 1927–2005. They filtered out the wells opened deeper than 100 m from the land surface or opened in a confined or mixed aquifer. They also filtered wells flagged with pumping, injection, obstructed, damaged, plugged, discontinued, dried, or flowing. We excluded Fan's wells with average WTDs larger than 300 m or smaller than 0 m and obtained 538,453 wells located within the *CONUS2* domain. We further excluded the wells of average WTDs larger than 100 m within the *CONUS1* domain and obtained 335,733 wells for comparison between *CONUS1* and *CONUS2*.

- **USGS streamflow (Figure 3b):** Similar to well observations, we directly collected daily observations during 1950–2000 from streamflow gauges using the USGS Daily Values Service. We removed the gauges following the steps in Maxwell et al. (2015): (1) gauges without drainage area reported, (2) gauges with drainage areas larger than 120% and smaller than 80% of the *CONUS2* drainage areas, and (3) gauges not mapped to or next to a ParFlow river cell. We also filtered missing values and then any gauges with less than ten observations. After filtering, we obtained average streamflow from 4,972 gauges located in *CONUS2* and 2,984 gauges located in *CONUS1*. The latter was used for the comparison between *CONUS1* and *CONUS2*.

- **National Hydrography Streamflow (Figure 3d):** More than 23,000 USGS stream gauges of daily observations during 1854–2004 have been mapped to the National Hydrography Dataset (NHD) by Stewart et al. (2006). After applying the same three-step filtering method described above (Maxwell et al., 2015), 8,120 and 5,150 gauges remained within the *CONUS2* and *CONUS1* domains, respectively. Each gauge record includes the mean and percentiles of the USGS daily streamflow for the period of record. We used the mean streamflow for the following analysis.

Of the four datasets listed here, the USGS WTD and streamflow datasets are raw observations without processing, so using them for model evaluation is the most direct approach. However, we also included Fan WTD and NHD streamflow to connect the evaluation of the *CONUS1* model completed by Maxwell et al. (2015). This allows us to directly evaluate model performance gains. Moreover, the use of USGS datasets allows us to customize the time interval and the number of observations for the calculations of mean values, which keeps the consistency with the long-term average state of the simulation results. As mentioned by Fan et al. (2007), 81% of the wells in their datasets have only one observation during 1927–2005, which is hard to ensure the representativeness of the long-term average state. Though our threshold of >10 observations may not be evenly distributed in 1950–2000, we tried our best to reduce the randomness represented by observations of a limited number while including as many wells/gauges as possible. All wells and gauges were mapped to the *CONUS2* domain for the following analysis. In cases where more than one well or gauge mapped to the same grid cell, we used their summed streamflow and averaged WTD values, respectively.

For every observation dataset, we calculated the RSR value for log-transformed WTD and streamflow. RSR is the ratio of root mean squared error (RMSE) to the standard deviation of the observations. We used log-transformed values to treat the variations at different scales equally. An RSR value of 1 suggests that the mean error equals the standard deviation of observations and good performance, while RSR values less than 0.5 suggest excellent simulation results (O'Neill et al., 2021).

3. Results

Figure 4 shows the WTD and streamflow simulated by the *CONUS2* model. Overall, we see shallow WTDs and denser stream networks in the eastern US. Clear basin and range systems rise in the western US. Streamflow networks form across multiple scales. Multi-scale variations of WTD are seen as well since even where we have regional deep WTDs, we see local ponding and shallow groundwater along streams. Figure 5 shows the difference in simulated WTD and streamflow between *CONUS1* and *CONUS2* at USGS wells and gauges, respectively, providing a general overview of the model differences. WTDs of *CONUS2* widely increase, yet we see decreased or less changed WTDs along streams, as exampled by the blue rectangle in Figure 5a. Broadly speaking, the range of WTD for *CONUS2* is much deeper (up to approximately 300 m) than in *CONUS1* (up to approximately 50 m). Streamflow generally decreases in the eastern US and increases in the western US, nested with a mixed pattern of both increase and decrease of the streamflow locally.

In the following sections, we conduct detailed evaluations of *CONUS1* and *CONUS2* compared to each other and to observations. We first evaluate the *CONUS2* performance relative to *CONUS1* by comparing the simulation results of both models to the four observation datasets listed in Section 2.4. To make these comparisons fair, unless otherwise noted, we perform them over *CONUS1* (i.e., the domain indicated by the dashed line box in Figure 1), as that is the area common to both simulations. Then we show the overall performance of the entire *CONUS2* domain, which extends to the coastal lines (Figure 1) and thus includes areas not discussed in *CONUS1* and *CONUS2* comparisons.

3.1 *CONUS1* and *CONUS2* comparisons

3.1.1 Hydraulic head

Hydraulic head is frequently used to evaluate large-scale groundwater models e.g., (Fan et al., 2013; Maxwell et al., 2015; Reinecke et al., 2020). However, hydraulic head comparisons may overestimate model performance because the high variability of land surface elevations may mask the true performance (Reinecke et al., 2020). As such, we present hydraulic head comparisons briefly here and focus most of our analysis on WTD comparisons in Section 3.1.2. The observed head here was calculated by subtracting the observed WTD from the processed land surface elevation. *CONUS1* and *CONUS2* used different DEMs and different topography processing approaches, resulting in different land surface elevations (see Section 2.1). Therefore, the observed heads of the two models are different even for the same observation dataset of WTD. In general, the heads of both CONUS models show high consistency with USGS and Fan datasets (Figure 6). Histograms using USGS and Fan datasets have different shapes because the Fan dataset has more samples of hydraulic heads around 300 m.

3.1.2 Water table depth

WTD is more important than hydraulic head for understanding interactions between groundwater and land-surface processes (Kollet and Maxwell, 2008; Maxwell and Condon, 2016) and the availability and accessibility of groundwater. Also, WTD comparisons are a more rigorous way of evaluating groundwater models because the land surface elevation is factored out, and only the residual of the hydraulic head is evaluated.

Figures 7a and b show WTD histograms of CONUS models with USGS and Fan observations, respectively. We see that *CONUS2* does a better job simulating deeper water tables than *CONUS1*. However, both models still overestimate the area with very shallow water tables. Few previous studies of large-scale groundwater modeling conducted a direct WTD comparison to observations due to many reasons, including model resolution and parameter uncertainty. Reinecke et al. (2020) conducted a comparison of the WTD performance for four global groundwater models with spatial resolution varying from 30″ (~900 m at the equator) to 6′ (~11 km at the equator). However, the points in his simulated vs. observed scatterplot did not form a positive correlation along the 1:1 line for all models. Here, while not a direct connection with the comparison in Reinecke et al. (2020), many of the evaluated points in the scatterplots (Figures 7c–f) fall along the 1:1 line, suggesting an improved WTD performance of CONUS models compared to prior modeling platforms. These improvements in performance may be due to the subsurface parameters used, the 3D nature of the simulation, the explicit treatment of the unsaturated zone, and the integrated surface water flow; all present in the *CONUS2* modeling platform.

In Figures 7c–f, points for evaluation identify two distinguishable subdomains of the entire comparison area. In the first subdomain (D1), points fall along the 1:1 line, indicating that CONUS models capture the real-world WTDs adequately, while in the second subdomain (D2), simulated WTDs cannot present the wide spectrum of observations. D1 and D2 points can be roughly separated by a horizontal line determined visually (red lines in Figure 7). The red lines indicate a WTD of 0.4 m for *CONUS1* and 0.1 m for *CONUS2*. We found that > 95% of D2 points in CONUS models by using either USGS or Fan observations are located on river cells in ParFlow. Figure 8 plots the WTD residuals (simulation values minus observation values) of CONUS models relative to USGS observations. Locations of D1 and D2 points are demonstrated in a small area indicated by the blue rectangle. Clearly, D2 points are distributed along streams for both models, especially in the regional groundwater convergence area, such as the eastern part of the exampled area. As a result, the poor model performance in the D2 subdomain should be attributed to the model resolution in these regions.

After removing D2 points, updated histograms in Figure 9 show improved WTD performance relative to that in Figures 7a–b, as the frequency of shallow water tables of CONUS models is largely reduced. Comparing Figure 10a with 10b or 10c with 10d, we see the obvious increase of WTD in *CONUS2* as the green area below the 1:1 line is reduced, showing a better fit to the 1:1 line. The spatial distribution of WTD increase is demonstrated in Figure 8 by the increased red areas of positive residuals. The example area in Figure 8 confirms that the WTD increase occurs in the D1 subdomain and illustrates that the WTD increase is more obvious on ridges than in valleys. However, we see the remaining green area below the 1:1 line in Figures 10b and d, which is also distributed in riparian areas as shown by D1 windows in Figure 8. This indicates the effects of model resolution in the D1 subdomain. Generally speaking, this suggests that the D1 subdomain represents areas where WTD is controlled by topography, recharge, and subsurface hydrostratigraphy. For a given model resolution, only these points might demonstrate improvement with traditional model calibration. The D2 subdomain, on the other hand, represents WTD values close to the streams and should only improve with increased resolution. However, given that the *CONUS2* model represents the D1 subdomain down to a very shallow WTD of 0.1 m, practically speaking, this should be sufficient to address many of the processes moderated by connections between shallow groundwater and surface processes e.g., (Fan et al., 2017; Keune et al., 2016; Kollet and Maxwell, 2008; Maxwell et al., 2007).

Quantitatively, the RSR value of log-transformed WTD for D1 points in the entire comparison area decreases from 1.58 to 1.36 by using the USGS dataset and from 1.68 to 1.33 by using the Fan dataset (see Table S2 in Supporting Information). In each HUC2 basin, D1 and D2 subdomains differentiating good and bad WTD performances are also observed (not shown here). RSR values for D1 points in HUC2 basins are plotted in Figures 10e–f and listed in Table S2. The decreased and less changed RSR values indicate the improved and comparable WTD performances of *CONUS2* relative to *CONUS1* in the eastern and western US, respectively. Generally, we see similar performances by using the USGS and Fan datasets.

3.1.3 Streamflow

Comparing the streamflow histograms of *CONUS2* with *CONUS1* (Figures 11a–b), the frequency of small values decreases while that of peak values increases, showing better consistency with observations. This improvement is also presented by scatterplots in Figures 11c–f. In *CONUS2*, the number of points falling below the 1:1 line is reduced, while a redder area is shown along the 1:1 line (Figures 11d and f), indicating the increased number of peak value points.

O'Neill et al. (2021) showed that discrepancies between simulated and observed streamflow in *CONUS1* are primarily affected by the differences between the drainage areas in *CONUS1* and the 'true' drainage areas determined by geospatial stream properties, showing a linearly proportional correlation between the two differences. In *CONUS2*, the drainage areas generated by our new topography processing were validated using the USGS drainage areas (Zhang et al., 2021), which should explain most of the improved streamflow performance. Other work in the new topography processing, such as the smoothing of river channels and the runoff simulations ensuring the connection of stream networks, may also contribute to the improved streamflow performance.

Quantitatively, a decrease in the RSR value of log-transformed streamflow from *CONUS1* to *CONUS2* in the entire comparison area is obtained by using either the USGS dataset (1.25 to 0.89) or the NHD dataset (1.11 to 0.77) (Table S2). We also observed the less scattered streamflow and the increased peak values from *CONUS1* to *CONUS2* in each HUC2 basin (not shown here). RSR values for HUC2 basins are plotted in Figures 11g–h and listed in Table S2. The decrease in the RSR value from *CONUS1* to *CONUS2* is seen for almost all HUC2 basins except for Texas Gulf, Rio Grande, and California due to the limited number of stream gauges. RSR values of streamflow of *CONUS2* are close to 0.5 in the first eight HUC2 basins, suggesting excellent streamflow performance of *CONUS2* in the eastern US. We didn't see obvious differences by using USGS and NHD datasets.

3.2 Performance of the entire *CONUS2* domain

WTD and streamflow performances of the entire *CONUS2* model extending to the coastal lines are shown in Figure 12. We see the two subdomains of WTD performance described in Section 3.1.2. 39,813 and 43,685 points are in D1 and D2, respectively, when using the USGS dataset (Figure 12a), while 244,688 and 293,765 points are in D1 and D2, respectively, when using the Fan dataset (Figure 12c). The extended areas of *CONUS2* relative to *CONUS1* (Figure 1) are mainly coastal areas with flat topography and shallow WTD. As mentioned in Section 3.1.2, riparian areas with shallow WTDs and strong heterogeneities are more sensitive to model resolutions. Hence the D2 points of the entire *CONUS2* model are largely explained by the increased coastal areas. For streamflow, the majority of data points fall closely along the 1:1 line, and only a small fraction of the points fall away from the 1:1 line. RSR values for WTD (D1 points) and streamflow of the entire *CONUS2* are 1.39 and 0.84 by using the USGS dataset and 1.33 and 0.74 by using the Fan and NHD datasets, which is comparable to the performances in the comparison area discussed in Section 3.1.

4. Discussion

As shown in Section 3, we see poor WTD performance due to model resolution in the D2 subdomain, which represents the groundwater convergence areas such as the riparian and coastal areas. In these areas, our model cannot capture the subgrid variations of topography gradient in 1 km grid cells, so most wells at local highlands near streams may be aggregated into river cells in ParFlow. Also, riparian areas with slight topography gradients are more sensitive to elevation aggregation, resulting in higher biases in simulation results which will mask the original small WTD values. In addition, riparian areas have strong subsurface heterogeneity, enhancing the sensitivity of performance to model resolution. However, wells are more located in riparian areas with shallow water tables, so the model performance is 'reduced' by the skewness of well locations towards riparian areas.

In the D1 subdomain, the increase of WTD in *CONUS2* mainly happens on ridges as opposed to valleys indicating the dominant factor here should be the improved subsurface configuration. It is also important to note that this is a pre-development simulation. For the remaining green area of smaller simulated WTDs in D1, pumping instead of pure monitoring in most of the wells, as mentioned by Maxwell et al. (2015), may also be an important factor in addition to model resolution. We see that the threshold of the D2 subdomain in *CONUS2* is compressed to < 0.1 m by the new topography processing. This is also a significant model improvement since the uncertainty of identifying poor model performance is reduced. Yet how to avoid too many D1 points swapped to the D2 subdomain with this compression, as happened in *CONUS2*, should be a focus in future work to improve the model performance further.

Obviously, the improved streamflow performance in *CONUS2* is largely attributed to the new topography processing. The remaining scattered streamflow of small values should be due to the significant uncertainties of small drainage areas, which again is attributed to the model resolution (Zhang et al., 2021). In addition, elevation aggregation at low resolution may drop the topographic potential for converging surface water and groundwater to local lowlands, resulting in smaller streamflow at small streams. Subsurface configuration may partly explain the smaller streamflow also. Our *CONUS2* subsurface tests (Tijerina-Kreuzer et al., 2023) show that the presence of flow barriers significantly improved the baseflow performance yet resulted in slightly smaller overall streamflow in both Upper Colorado River Basin and Delaware-Susquehanna Basin.

The improved WTD and streamflow performances confirm that our new subsurface configuration and topography processing are effective, suggesting a new workflow for the community of large-scale groundwater or integrated hydrologic modeling. Our work also highlights that resolution is not always the key issue to improving the performance of large-scale groundwater models, strengthening the conclusion of Reinecke et al. (2020). The CONUS models have the same 1 km resolution but have varying performances due to the different subsurface configurations and topography processing. This emphasizes that the community should be cautious about configuring the subsurface and topography at low resolution, which should be representative of most of the subgrid variations, instead of pursuing the higher resolution only.

5. Summary and Conclusions

The ParFlow CONUS model is a continental-scale, integrated surface-water and groundwater modeling platform. The first version, ParFlow CONUS 1.0, made significant contributions to the community of large-scale hydrologic modeling. In this study, we introduce the latest version, ParFlow CONUS 2.0, which includes enhancements in topography processing and subsurface configuration. We performed steady-state simulations using this model, in which we leveraged GPU acceleration. We evaluated *CONUS2* performance using multi-source observations by comparing the simulated water table depth (WTD) and streamflow to *CONUS1*.

Both CONUS models show good correlations between simulated and observed WTDs and perform better than previous large-scale groundwater models. Here we differentiate two subdomains of model performance (referred to as D1 and D2). Wells in the D2 subdomain are generally located in groundwater convergent zones where poor performance can be attributed to the 1 km spatial resolution of our model, which is unable to consistently resolve subgrid variations around streams. If we exclude the D2 wells from our analysis, we show that the performance of D1 is quite good and, furthermore, that the performance has improved from the *CONUS1* to the *CONUS2* model. Another improvement is that the threshold between D1 and D2 is reduced from 0.4 m of *CONUS1* to 0.1 m of *CONUS2*. Streamflow performance is also improved in the *CONUS2* model. This increased performance is likely due to the improved topographic processing that leads to better agreement between the model topography and reported stream gauge drainage areas.

The WTD performance of the *CONUS2* model is better in the western US, where there are deeper water tables and less local convergence. Whereas the streamflow performance is good over the entire *CONUS2* and is excellent in the eastern US. These eastern areas are challenging for WTD performance due to their flat topography and high subsurface heterogeneity, both of which are sensitive to aggregations at the 1 km model resolution. Future work to improve the performance of CONUS models should focus on the topography processing of coastal areas or flat groundwater convergence areas.

The changes from *CONUS1* to *CONUS2* highlight the improvements in model performance that can be achieved even without increasing spatial resolution. It is interesting to note that *CONUS1* and *CONUS2* models show different performances for both WTD and streamflow though they have the same spatial resolution of 1 km. The improved performance of *CONUS2* suggests that the improvements to topography and the subsurface parameter values and structure were valuable and may outweigh other model improvements, such as increased resolution. These somewhat counterintuitive findings might help guide the hydrology community in future modeling work. The improved WTD and streamflow performance of *CONUS2* are encouraging and demonstrate the effectiveness of the newly developed subsurface configuration and topography processing. As an integrated hydrology model, the *CONUS2* model will be a promising platform for future applications and extensions to address large-scale water resource questions.

Acknowledgments

This research has been supported by the U.S. Department of Energy Office of Science (DE-AC02-05CH11231) and the US National Science Foundation Office of Advanced Cyberinfrastructure (OAC- 2054506 and OAC-1835855). We are pleased to acknowledge that the work reported on in this paper was substantially performed using the Princeton Research Computing resources at Princeton University which is consortium of groups led by the Princeton Institute for Computational Science and Engineering (PICSciE) and

Office of Information Technology's Research Computing. We would like to acknowledge high-performance computing support from Cheyenne (doi:10.5065/D6RX99HX) provided by NCAR's Computational and Information Systems Laboratory, sponsored by the National Science Foundation. Datasets will be made available via the HydroFrame project (https://hydroframe.org) upon final publication. The authors declare no conflict of interest.

References

Ashby, S.F., Falgout, R.D., 1996. A parallel multigrid preconditioned conjugate gradient algorithm for groundwater flow simulations. Nucl Sci Eng, 124(1): 145-159.

CCRS/CCMEO/NRCan, CONABIO, CONAFOR, INEGI, USGS, 2020. 2015 Land Cover of North America at 30 meters. In: CCRS/CCMEO/NRCan et al. (Eds.), Ottawa, Ontario, Canada Sioux Falls, South Dakota, USA Mexico City, México San Juan de Ocotán, Jalisco, México Aguascalientes, México Montréal, Québec, Canada.

Chow, V.T., Maidment, D.R., Mays, L.W., 1988. Applied hydrology. McGraw-Hill series in water resources and environmental engineering. McGraw-Hill, New York, xiii, 572 p. pp.

Clark, M.P. et al., 2015. Improving the representation of hydrologic processes in Earth System Models. Water Resour Res, 51(8): 5929-5956. DOI:https://doi.org/10.1002/2015WR017096

Computational and Information Systems Laboratory, 2019. Cheyenne: HPE/SGI ICE XA System (University Community Computing). Boulder, CO: National Center for Atmospheric Research. DOI:10.5065/D6RX99HX

Condon, L.E., Atchley, A.L., Maxwell, R.M., 2020a. Evapotranspiration depletes groundwater under warming over the contiguous United States. Nat Commun, 11(1): 873. DOI:10.1038/s41467-020-14688-0

Condon, L.E. et al., 2021. Global Groundwater Modeling and Monitoring: Opportunities and Challenges. Water Resour Res, 57(12): e2020WR029500. DOI:https://doi.org/10.1029/2020WR029500

Condon, L.E. et al., 2020b. Where Is the Bottom of a Watershed? Water Resour Res, 56(3).

Condon, L.E., Maxwell, R.M., 2019a. Modified priority flood and global slope enforcement algorithm for topographic processing in physically based hydrologic modeling applications. Computers & Geosciences, 126: 73-83. DOI:10.1016/j.cageo.2019.01.020

Condon, L.E., Maxwell, R.M., 2019b. Simulating the sensitivity of evapotranspiration and streamflow to large-scale groundwater depletion. Sci Adv, 5(6). DOI:ARTN eaav457410.1126/sciadv.aav4574

Dai, Y. et al., 2019a. A review of the global soil property maps for Earth system models. SOIL, 5(2): 137-158. DOI:10.5194/soil-5-137-2019

Dai, Y. et al., 2019b. A Global High-Resolution Data Set of Soil Hydraulic and Thermal Properties for Land Surface Modeling. J Adv Model Earth Sy, 11(9): 2996-3023. DOI:https://doi.org/10.1029/2019MS001784

de Graaf, I.E.M., Sutanudjaja, E.H., van Beek, L.P.H., Bierkens, M.F.P., 2015. A high-resolution global-scale groundwater model. Hydrol Earth Syst Sc, 19(2): 823-837. DOI:10.5194/hess-19-823-2015

de Graaf, I.E.M. et al., 2017. A global-scale two-layer transient groundwater model: Development and application to groundwater depletion. Advances in Water Resources, 102: 53-67. DOI:https://doi.org/10.1016/j.advwatres.2017.01.011

Fan, Y., 2015. Groundwater in the Earth's critical zone: Relevance to large-scale patterns and processes. Water Resour Res, 51(5): 3052-3069.

Fan, Y. et al., 2019. Hillslope Hydrology in Global Change Research and Earth System Modeling. Water Resour Res, 55(2): 1737-1772. DOI:10.1029/2018wr023903

Fan, Y., Li, H., Miguez-Macho, G., 2013. Global Patterns of Groundwater Table Depth. Science, 339(6122): 940-943. DOI:10.1126/science.1229881

Fan, Y., Miguez-Macho, G., Jobbágy, E.G., Jackson, R.B., Otero-Casal, C., 2017. Hydrologic regulation of plant rooting depth. Proceedings of the National Academy of Sciences, 114(40): 10572-10577. DOI:10.1073/pnas.1712381114

Fan, Y., Miguez-Macho, G., Weaver, C.P., Walko, R., Robock, A., 2007. Incorporating water table dynamics in climate modeling: 1. Water table observations and equilibrium water table simulations. Journal of Geophysical Research: Atmospheres, 112(D10). DOI:https://doi.org/10.1029/2006JD008111

Ferguson, G. et al., 2023. Groundwater deeper than 500 m contributes less than 0.1% of global river discharge. Commun Earth Environ, 4(1): 48. DOI:10.1038/s43247-023-00697-6

Foster, L., Maxwell, R., 2019. Sensitivity analysis of hydraulic conductivity and Manning's n parameters lead to new method to scale effective hydraulic conductivity across model resolutions. Hydrol Process, 33(3): 332-349. DOI:10.1002/hyp.13327

Gleeson, T., Befus, K.M., Jasechko, S., Luijendijk, E., Cardenas, M.B., 2016. The global volume and distribution of modern groundwater. Nat Geosci, 9(2): 161-+. DOI:10.1038/Ngeo2590

Gleeson, T., Moosdorf, N., Hartmann, J., van Beek, L.P.H., 2014. A glimpse beneath earth's surface: GLobal HYdrogeology MaPS (GLHYMPS) of permeability and porosity. Geophys Res Lett, 41(11): 3891-3898. DOI:10.1002/2014gl059856

Gleeson, T. et al., 2011. Mapping permeability over the surface of the Earth. Geophys Res Lett, 38. DOI:Artn L0240110.1029/2010gl045565

Gleeson, T. et al., 2021. GMD perspective: The quest to improve the evaluation of groundwater representation in continental- to global-scale models. Geosci. Model Dev., 14(12): 7545-7571. DOI:10.5194/gmd-14-7545-2021

Gochis, D.J., Yu, W., Yates, D.N., 2015. The WRF-Hydro model technical description and user's guide, version 3.0. NCAR Technical Document, 120 pages.

Hokkanen, J. et al., 2021. Leveraging HPC accelerator architectures with modern techniques — hydrologic modeling on GPUs with ParFlow. Computat Geosci, 25(5): 1579-1590. DOI:10.1007/s10596-021-10051-4

Huscroft, J., Gleeson, T., Hartmann, J., Börker, J., 2018. Compiling and Mapping Global Permeability of the Unconsolidated and Consolidated Earth: GLobal HYdrogeology MaPS 2.0 (GLHYMPS 2.0). Geophys Res Lett, 45(4): 1897-1904. DOI:https://doi.org/10.1002/2017GL075860

Jones, J.E., Woodward, C.S., 2000. Preconditioning Newton-Krylov methods for variably saturated flow. Computational Methods in Water Resources, Vols 1 and 2: 101-106.

Jones, J.E., Woodward, C.S., 2001. Newton-Krylov-multigrid solvers for large-scale, highly heterogeneous, variably saturated flow problems. Advances in Water Resources, 24(7): 763-774. DOI:Doi 10.1016/S0309-1708(00)00075-0

Keune, J. et al., 2016. Studying the influence of groundwater representations on land surface-atmosphere feedbacks during the European heat wave in 2003. J Geophys Res-Atmos, 121(22): 13301-13325. DOI:10.1002/2016jd025426

Kollet, S.J., Maxwell, R.M., 2006. Integrated surface-groundwater flow modeling: A free-surface overland flow boundary condition in a parallel groundwater flow model. Advances in Water Resources, 29(7): 945-958.

Kollet, S.J., Maxwell, R.M., 2008. Capturing the influence of groundwater dynamics on land surface processes using an integrated, distributed watershed model. Water Resour Res, 44(2). DOI:Artn W0240210.1029/2007wr006004

Kollet, S.J. et al., 2010. Proof of concept of regional scale hydrologic simulations at hydrologic resolution utilizing massively parallel computer resources. Water Resour Res, 46. DOI:Artn W0420110.1029/2009wr008730

Livneh, B. et al., 2015. A spatially comprehensive, hydrometeorological data set for Mexico, the U.S., and Southern Canada 1950–2013. Sci Data, 2(1): 150042. DOI:10.1038/sdata.2015.42

Maurer, E.P., Wood, A.W., Adam, J.C., Lettenmaier, D.P., Nijssen, B., 2002. A Long-Term Hydrologically Based Dataset of Land Surface Fluxes and States for the Conterminous United States. J Climate, 15(22): 3237-3251. DOI:10.1175/1520-0442(2002)015<3237:ALTHBD>2.0.CO;2

Maxwell, R.M., 2013. A terrain-following grid transform and preconditioner for parallel, large-scale, integrated hydrologic modeling. Advances in Water Resources, 53: 109-117. DOI:https://doi.org/10.1016/j.advwatres.2012.10.001

Maxwell, R.M., Chow, F.K., Kollet, S.J., 2007. The groundwater–land-surface–atmosphere connection: Soil moisture effects on the atmospheric boundary layer in fully-coupled simulations. Advances in Water Resources, 30(12): 2447-2466. DOI:https://doi.org/10.1016/j.advwatres.2007.05.018

Maxwell, R.M., Condon, L.E., 2016. Connections between groundwater flow and transpiration partitioning. Science, 353(6297): 377-380.

Maxwell, R.M., Condon, L.E., Kollet, S.J., 2015. A high-resolution simulation of groundwater and surface water over most of the continental US with the integrated hydrologic model ParFlow v3. Geosci Model Dev, 8(3): 923-937. DOI:10.5194/gmd-8-923-2015

Maxwell, R.M. et al., 2016. The imprint of climate and geology on the residence times of groundwater. Geophys Res Lett, 43(2): 701-708. DOI:10.1002/2015gl066916

Maxwell, R.M. et al., 2014. Surface-subsurface model intercomparison: A first set of benchmark results to diagnose integrated hydrology and feedbacks. Water Resour Res, 50(2): 1531-1549. DOI:https://doi.org/10.1002/2013WR013725

McIntosh, J.C., Ferguson, G., 2021. Deep Meteoric Water Circulation in Earth's Crust. Geophys Res Lett, 48(5).

Müller Schmied, H. et al., 2021. The global water resources and use model WaterGAP v2.2d: model description and evaluation. Geosci. Model Dev., 14(2): 1037-1079. DOI:10.5194/gmd-14-1037-2021

Naz, B.S., Sharples, W., Ma, Y., Goergen, K., Kollet, S., 2023. Continental-scale evaluation of a fully distributed coupled land surface and groundwater model, ParFlow-CLM (v3.6.0), over Europe. Geosci. Model Dev., 16(6): 1617-1639. DOI:10.5194/gmd-16-1617-2023

O'Neill, M.M.F., Tijerina, D.T., Condon, L.E., Maxwell, R.M., 2021. Assessment of the ParFlow–CLM CONUS 1.0 integrated hydrologic model: evaluation of hyper-resolution water balance components across the contiguous United States. Geosci. Model Dev., 14(12): 7223-7254. DOI:10.5194/gmd-14-7223-2021

Osei-Kuffuor, D., Maxwell, R.M., Woodward, C.S., 2014. Improved numerical solvers for implicit coupling of subsurface and overland flow. Advances in Water Resources, 74: 185-195. DOI:https://doi.org/10.1016/j.advwatres.2014.09.006

ParFlow developers, 2022. parflow/parflow: ParFlow Version 3.11.0 (v3.11.0) [Software]. Zenodo. DOI:https://doi.org/10.5281/zenodo.7055486

Reinecke, R. et al., 2019. Challenges in developing a global gradient-based groundwater model (G3M v1.0) for the integration into a global hydrological model. Geosci. Model Dev., 12(6): 2401-2418. DOI:10.5194/gmd-12-2401-2019

Reinecke, R. et al., 2020. Importance of Spatial Resolution in Global Groundwater Modeling. Groundwater, 58(3): 363-376. DOI:https://doi.org/10.1111/gwat.12996

Richards, L.A., 1931. CAPILLARY CONDUCTION OF LIQUIDS THROUGH POROUS MEDIUMS. Physics, 1(5): 318-333. DOI:10.1063/1.1745010

Scanlon, B.R. et al., 2023. Global water resources and the role of groundwater in a resilient water future. Nature Reviews Earth & Environment. DOI:10.1038/s43017-022-00378-6

Schaap, M.G., Leij, F.J., 1998. Database-related accuracy and uncertainty of pedotransfer functions. Soil science, v. 163(no. 10): pp. 765-779-1998 v.163 no.10. DOI:10.1097/00010694-199810000-00001

Shangguan, W., Dai, Y., Duan, Q., Liu, B., Yuan, H., 2014. A global soil data set for earth system modeling. J Adv Model Earth Sy, 6(1): 249-263. DOI:https://doi.org/10.1002/2013MS000293

Shangguan, W., Hengl, T., de Jesus, J.M., Yuan, H., Dai, Y.J., 2017. Mapping the global depth to bedrock for land surface modeling. J Adv Model Earth Sy, 9(1): 65-88.

Stewart, D.W., Rea, A., Wolock, D.M., 2006. USGS Streamgages Linked to the Medium Resolution NHD. 195. DOI:10.3133/ds195

Swilley, J. et al., 2023. Continental scale hydrostratigraphy: comparing datasets to analytical solutions. Groundwater, Under Review.

Tijerina, D. et al., 2021. Continental Hydrologic Intercomparison Project, Phase 1: A Large-Scale Hydrologic Model Comparison Over the Continental United States. Water Resour Res, 57(7): e2020WR028931. DOI:https://doi.org/10.1029/2020WR028931

Tijerina-Kreuzer, D. et al., 2023. Continental scale hydrostratigraphy: testing alternate data-driven approaches. Groundwater, Under Review.

Tran, H. et al., 2022. A hydrological simulation dataset of the Upper Colorado River Basin from 1983 to 2019. Sci Data, 9(1).

Verkaik, J., Sutanudjaja, E.H., Oude Essink, G.H.P., Lin, H.X., Bierkens, M.F.P., 2022. GLOBGM v1.0: a parallel implementation of a 30 arcsec PCR-GLOBWB-MODFLOW global-scale groundwater model. Geosci. Model Dev. Discuss., 2022: 1-27. DOI:10.5194/gmd-2022-226

Yang, C., Maxwell, R.M., Valent, R., 2022. Accelerating the Lagrangian simulation of water ages on distributed, multi-GPU platforms: The importance of dynamic load balancing. Computers & Geosciences, 166: 105189. DOI:https://doi.org/10.1016/j.cageo.2022.105189

Yang, C. et al., 2021. Accelerating the Lagrangian particle tracking of residence time distributions and source water mixing towards large scales. Computers & Geosciences, 151.

Zhang, J., Condon, L.E., Tran, H., Maxwell, R.M., 2021. A national topographic dataset for hydrological modeling over the contiguous United States. Earth Syst. Sci. Data, 13(7): 3263-3279. DOI:10.5194/essd-13-3263-2021

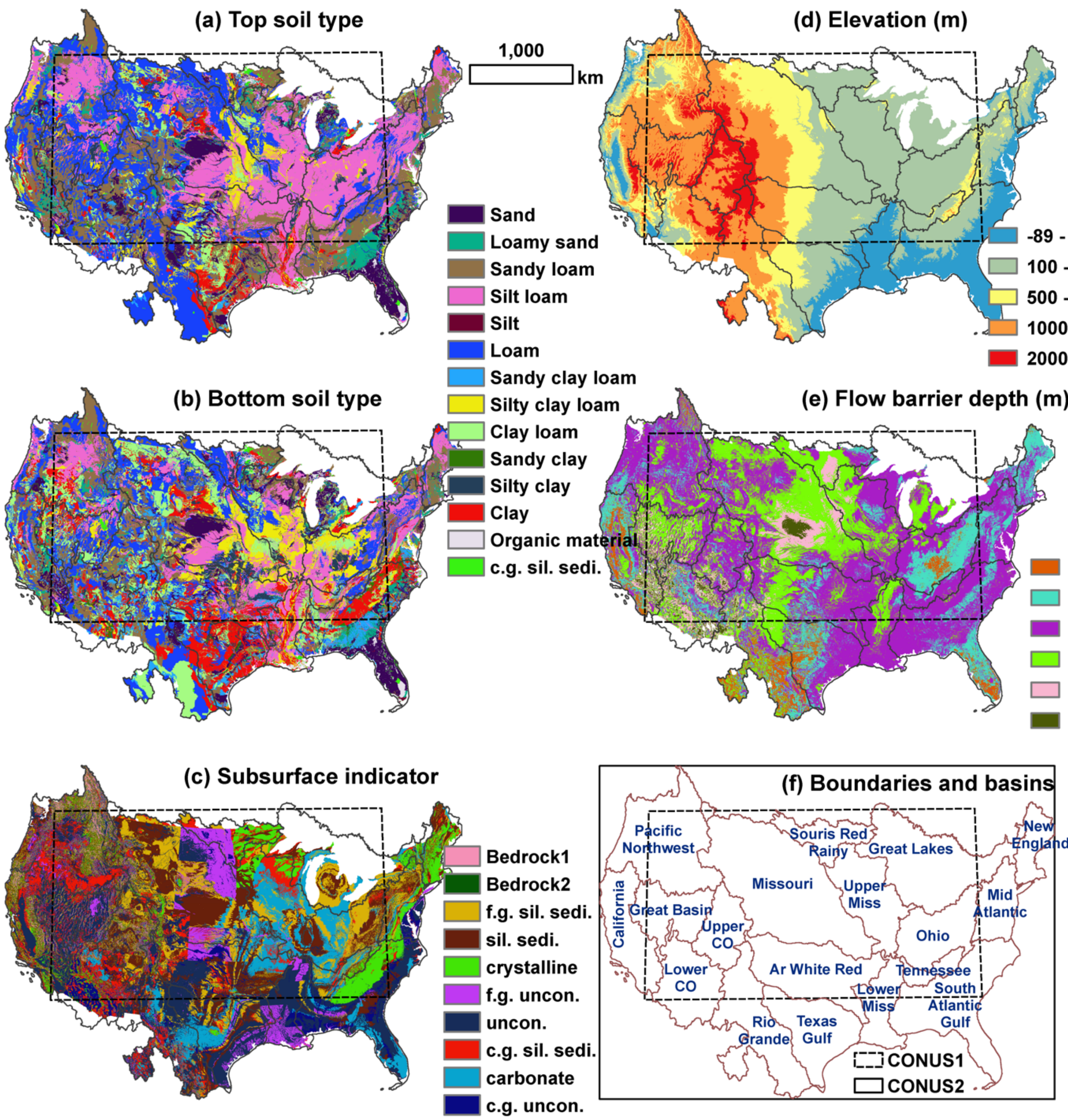

Figure 1. Maps of topsoil type (0–1m) (a), bottom soil type (1–2m) (b), geologic unit (c), elevation (m a.s.l.) (d), depth of flow barrier (e), and boundaries of CONUS models and HUC2 basins (f). (c) shows the top geologic units (i.e., those in the 5 m layer), for example, and other layers are shown in supporting information (Figure S1). c.g., f.g., sil., sedi., uncon. refer to coarse-grained, fine-grained, siliciclastic, sedimentary, and unconsolidated, respectively.

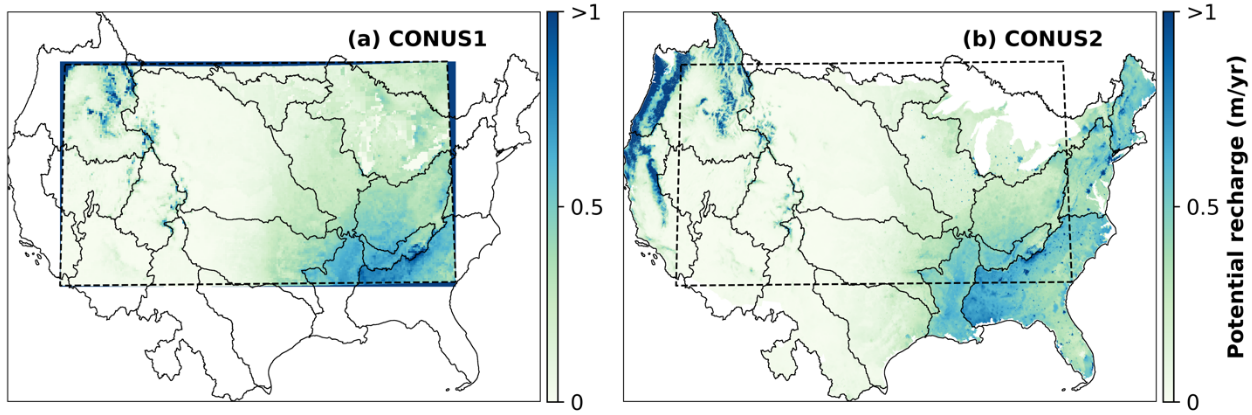

Figure 2. Comparison of potential recharge between the CONUS1 and CONUS2 domains.

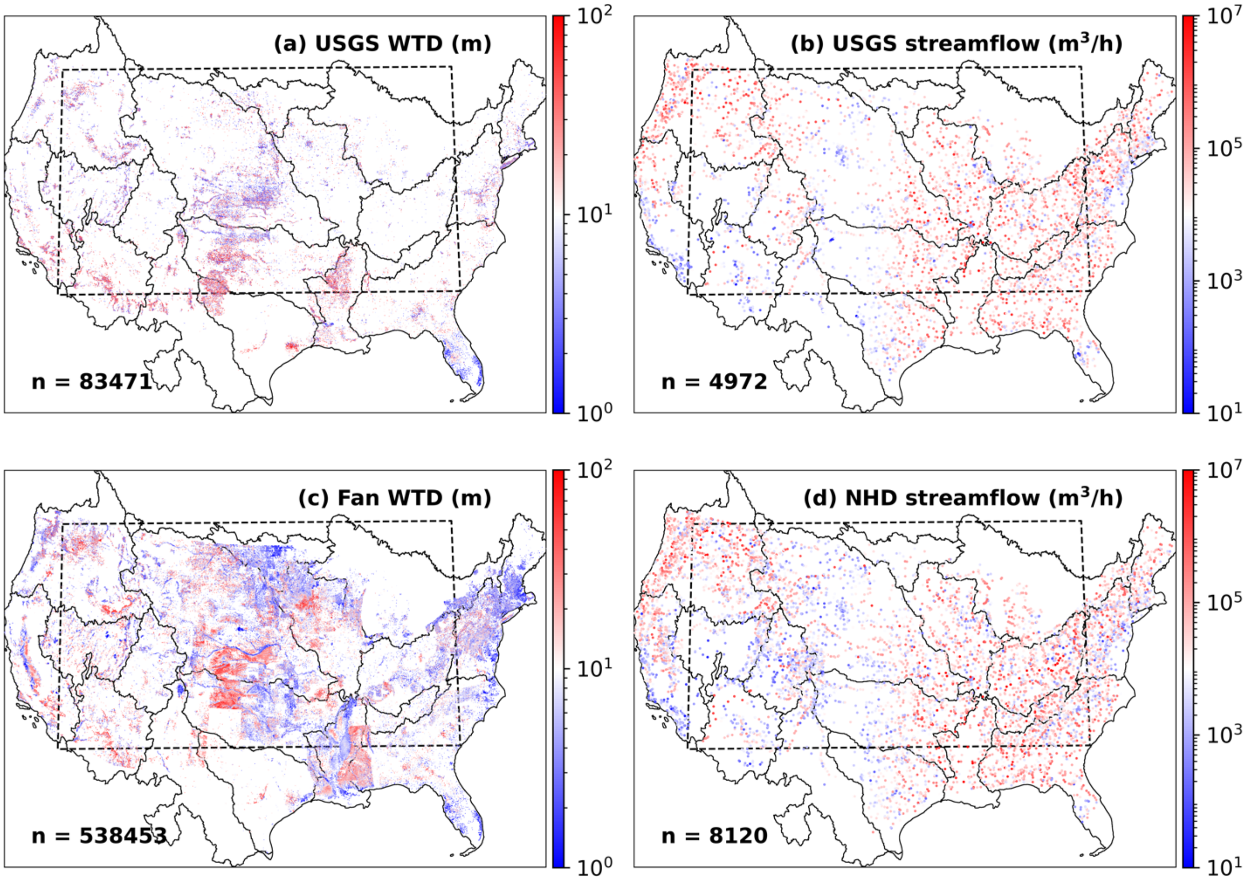

Figure 3. Observed water table depth and streamflow used for model evaluation.

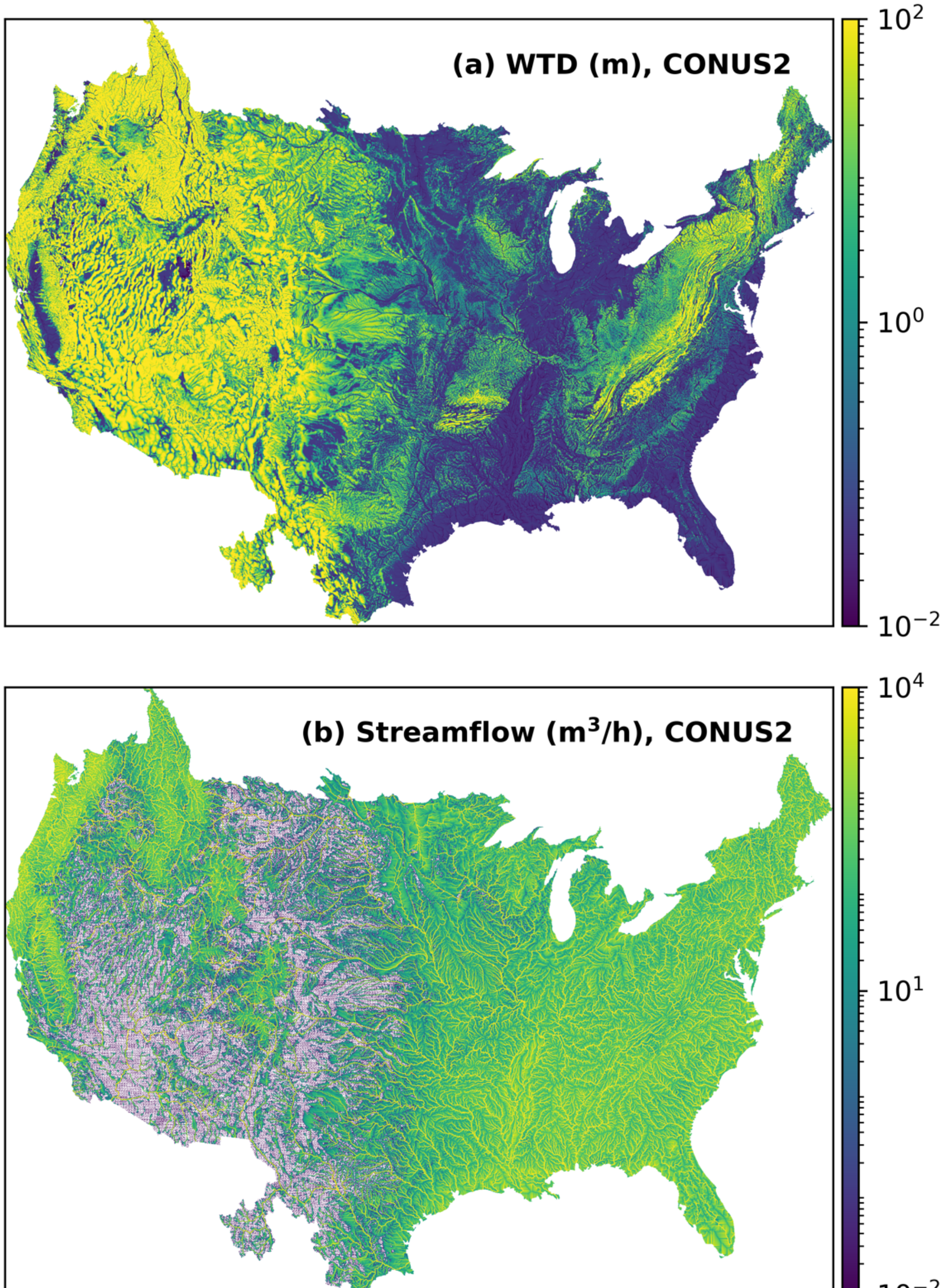

Figure 4. Water table depth (WTD) and streamflow simulated by CONUS2.

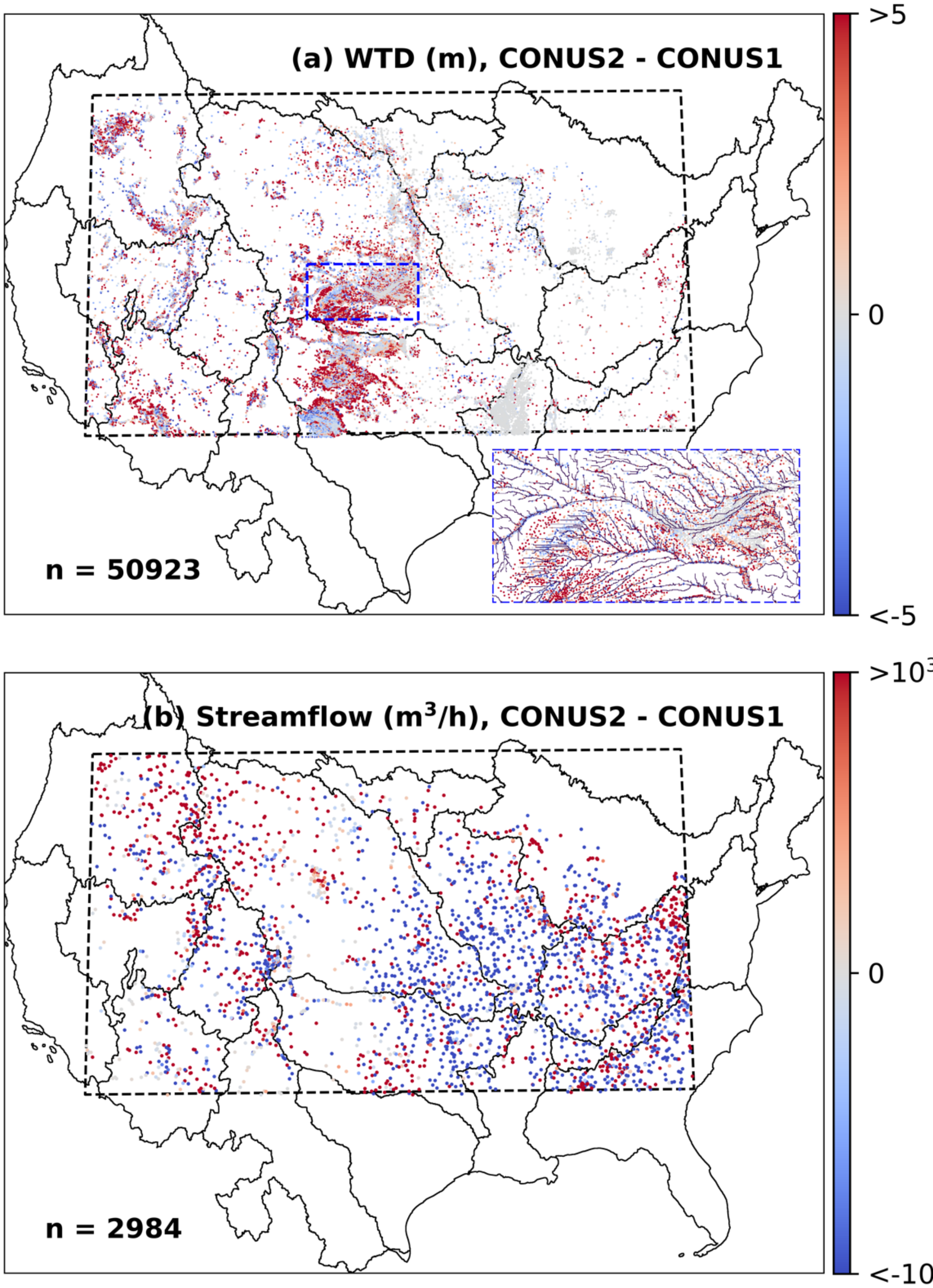

Figure 5. Difference of simulated water table depth (WTD) and streamflow between CONUS1 and CONUS2 at USGS wells and gauges, respectively.

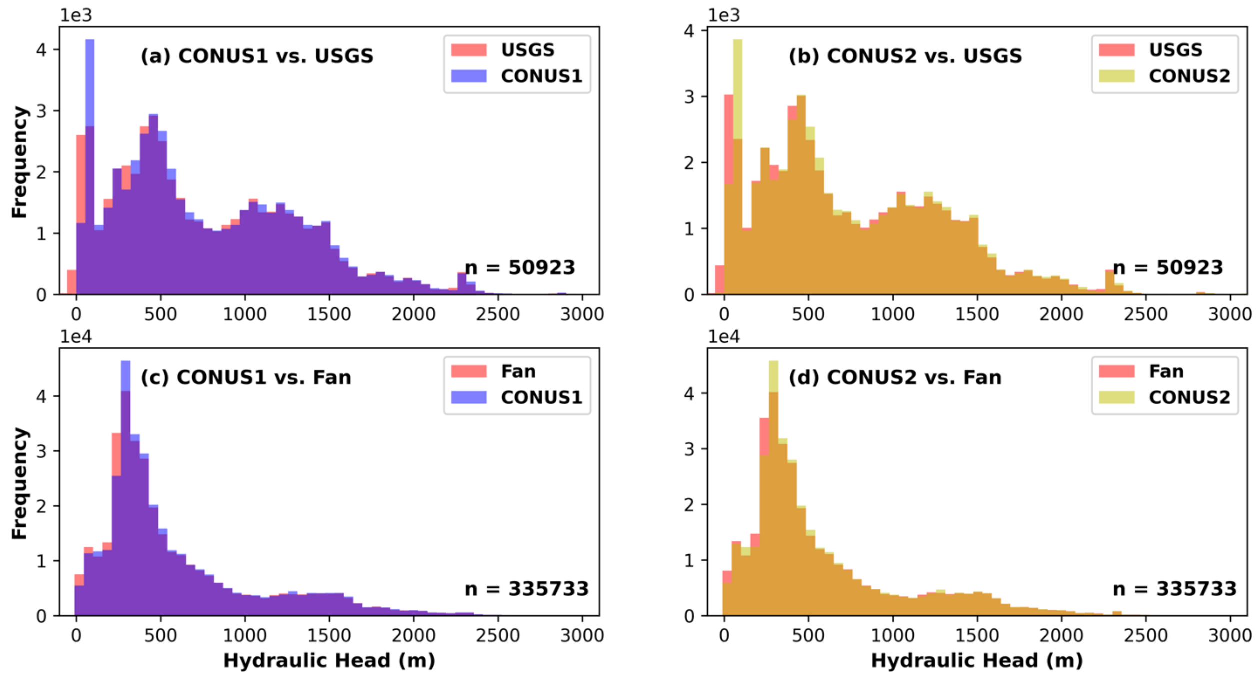

Figure 6. Comparison of the simulated hydraulic head with observations.

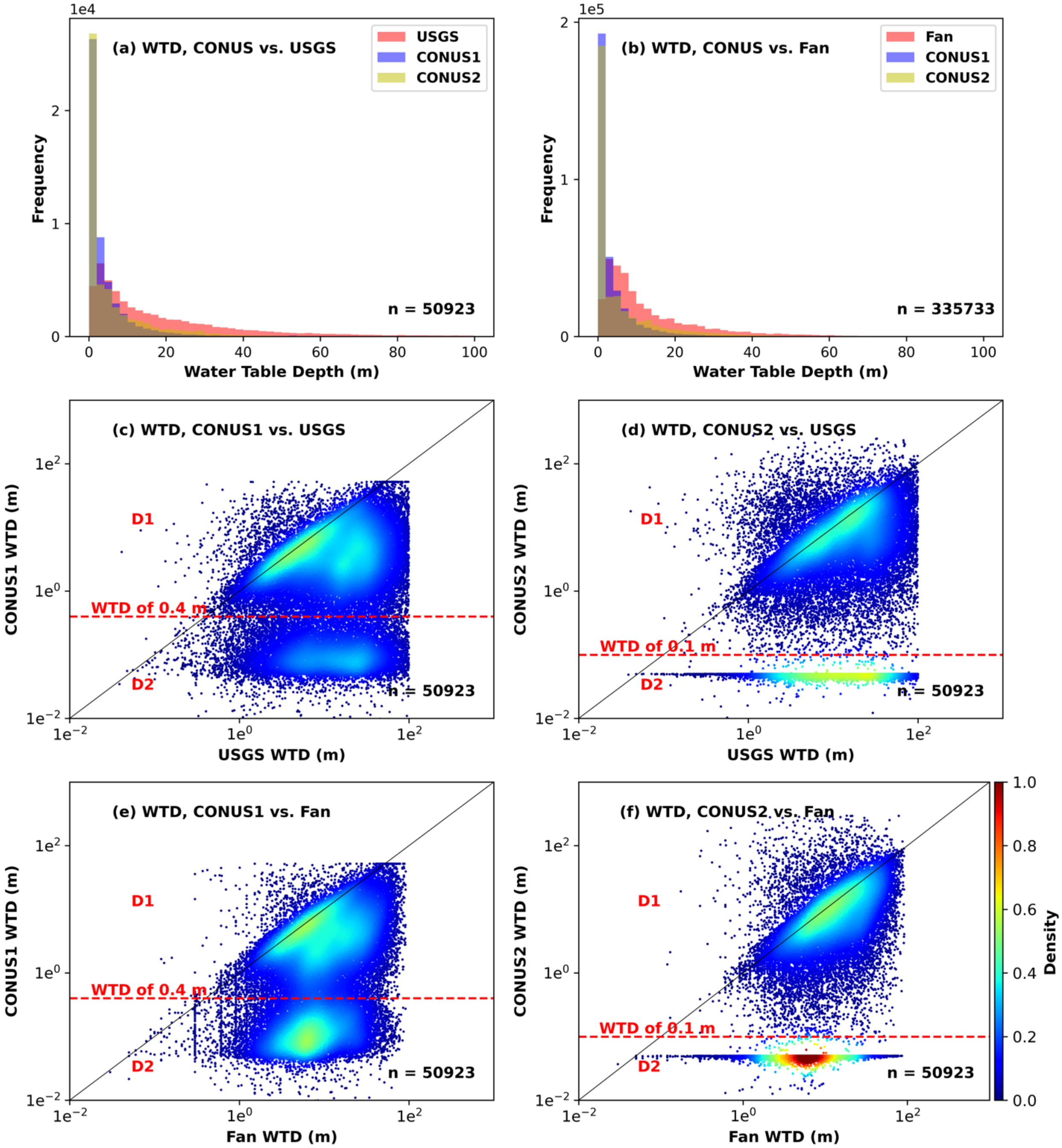

Figure 7. Histograms (a–b) and scatterplots (c–f) of simulated vs. observed water table depth (WTD). (e–f) are plotted using random samples of the Fan dataset.

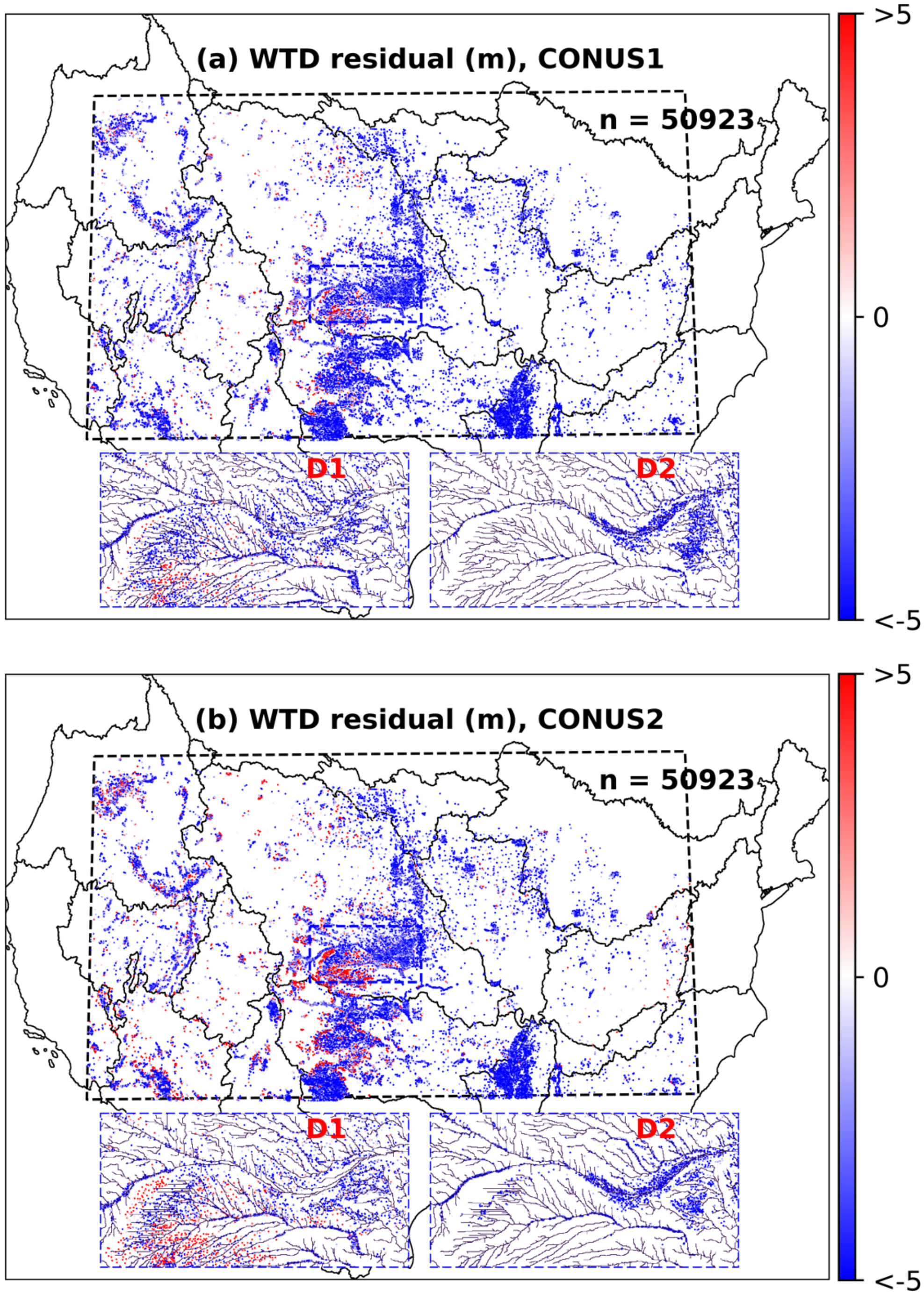

Figure 8. WTD residuals of CONUS1 and CONUS2 by comparing with USGS observations. D1 and D2 points are shown for the selected area indicated by the blue rectangle.

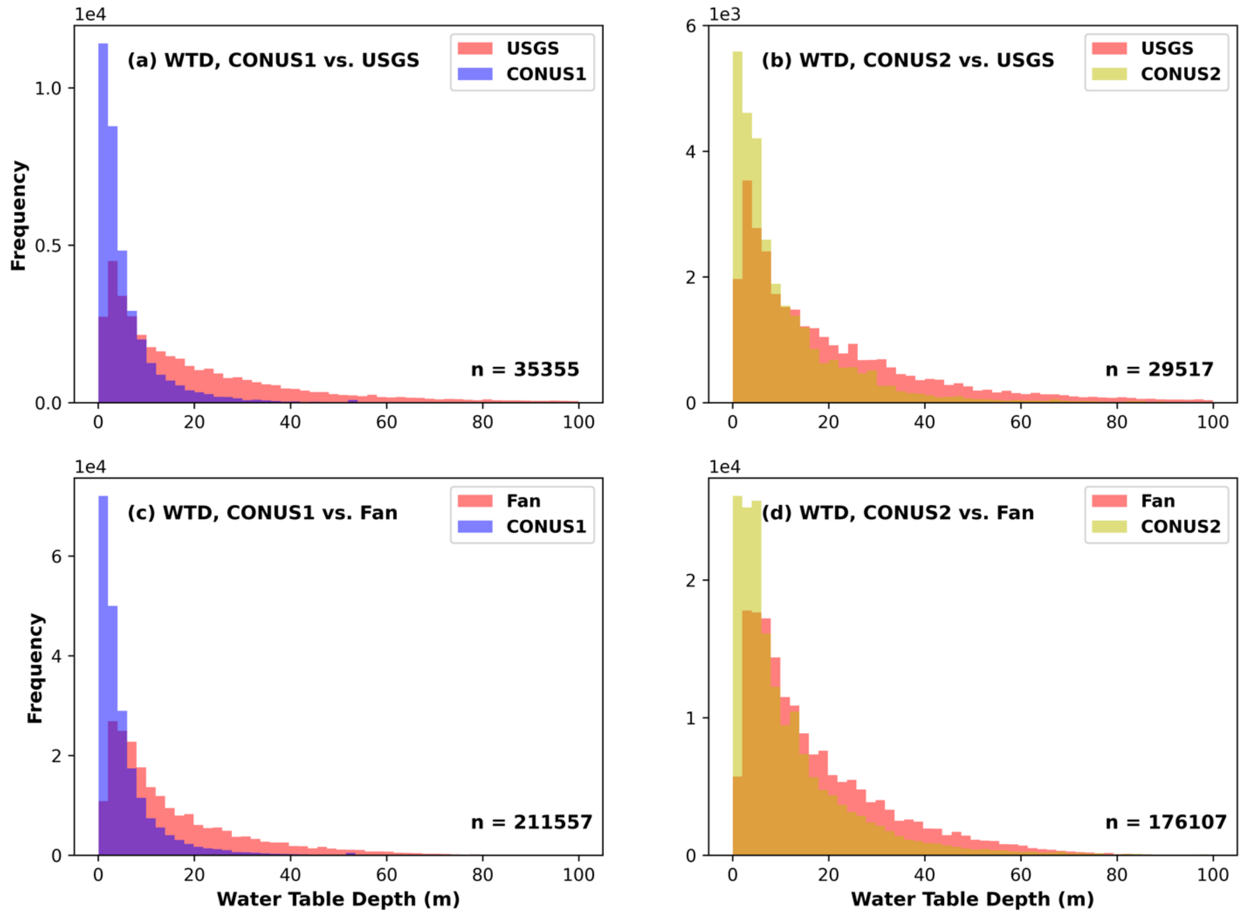

Figure 9. Histograms of water table depth (WTD) for D1 points.

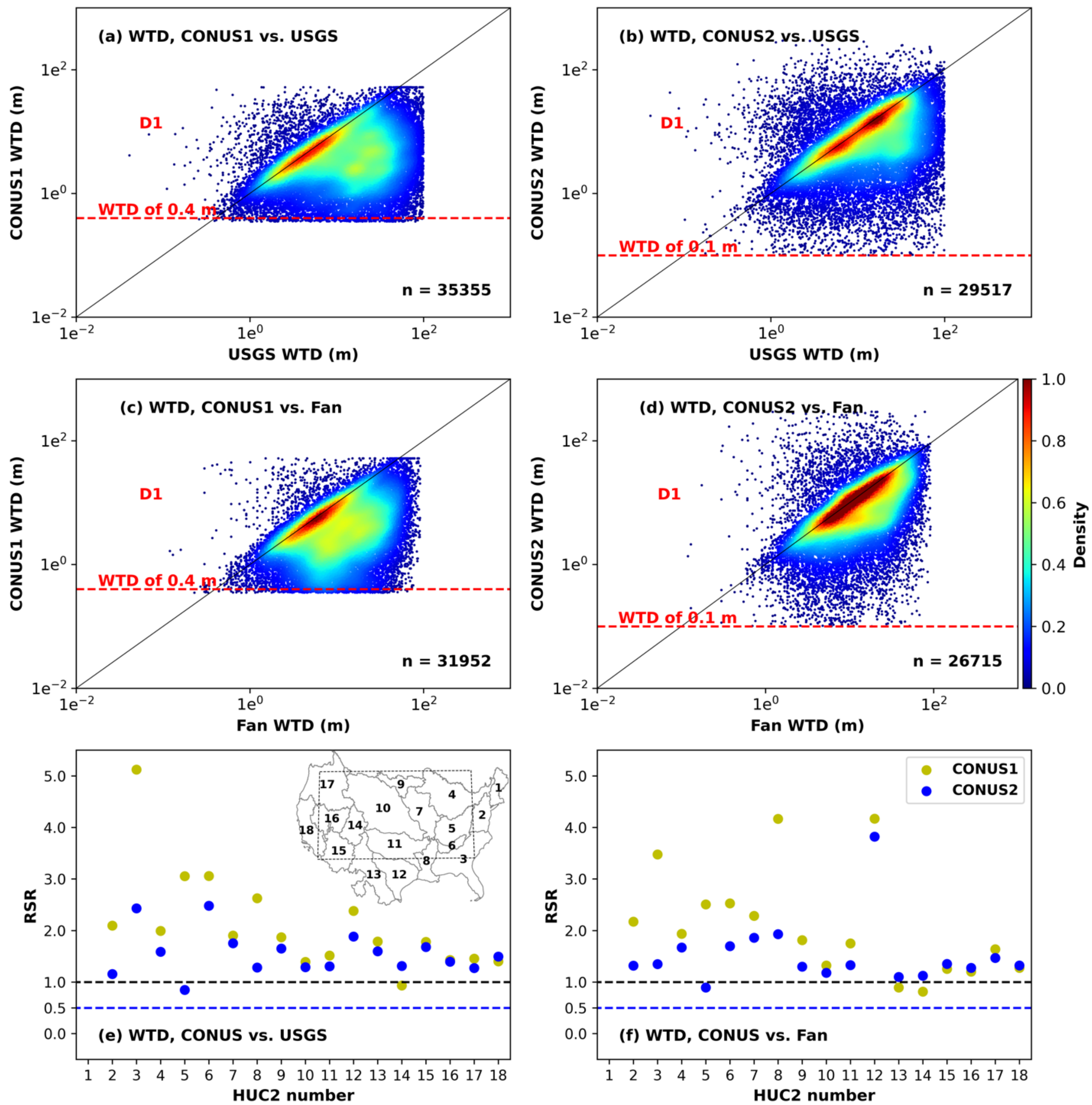

Figure 10. Scatterplots of simulated vs. observed water table depth (WTD) for D1 points (a–d), and RSR values of log-transformed WTDs of D1 points by HUC2 basin (e–f). (c–d) are obtained by removing D2 in Figures 7e–f.

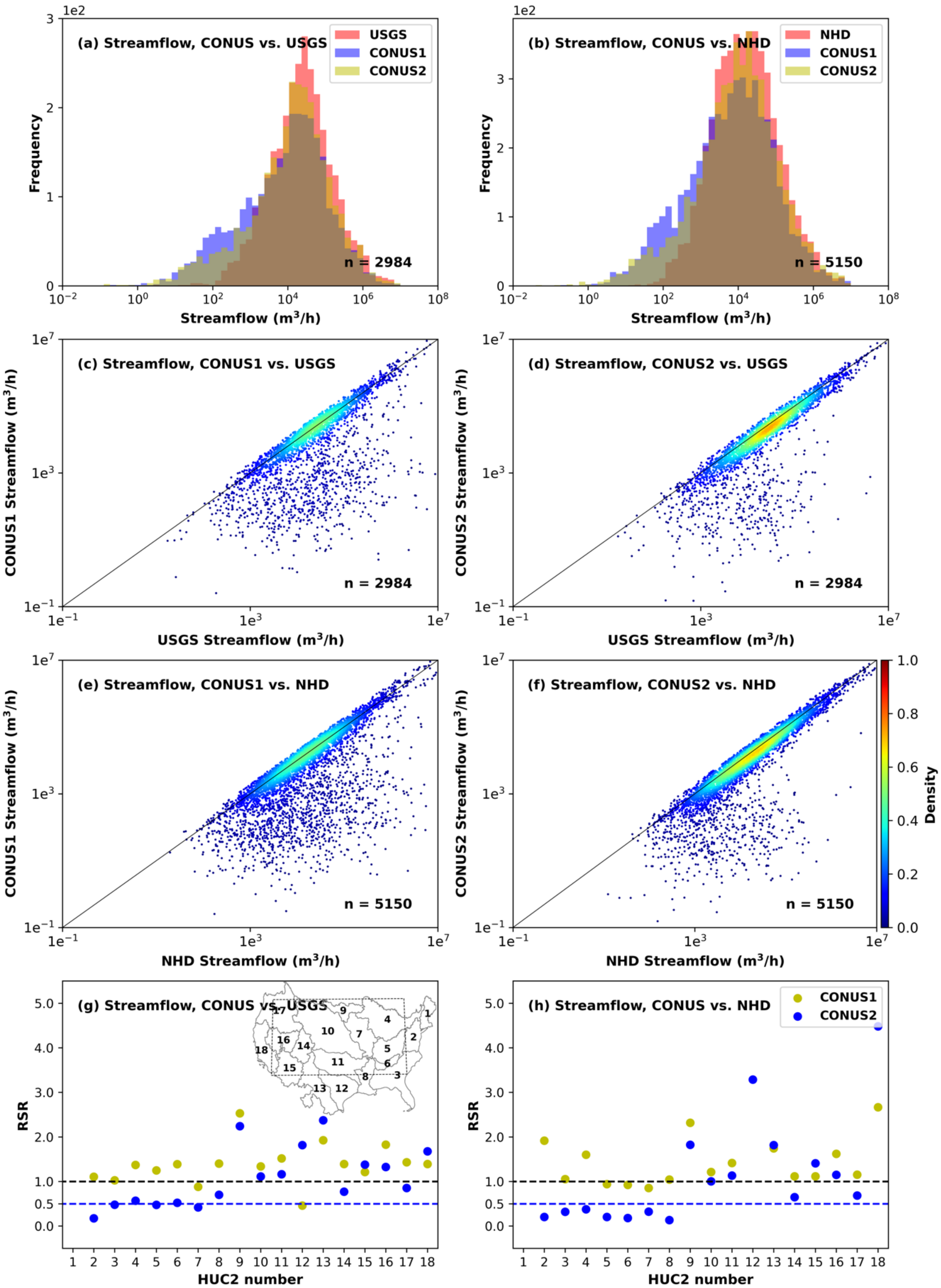

Figure 11. Histograms (a–b) and scatterplots (c–f) of simulated vs. observed streamflow, and RSR values of log-transformed streamflow by HUC2 basin (g–h).

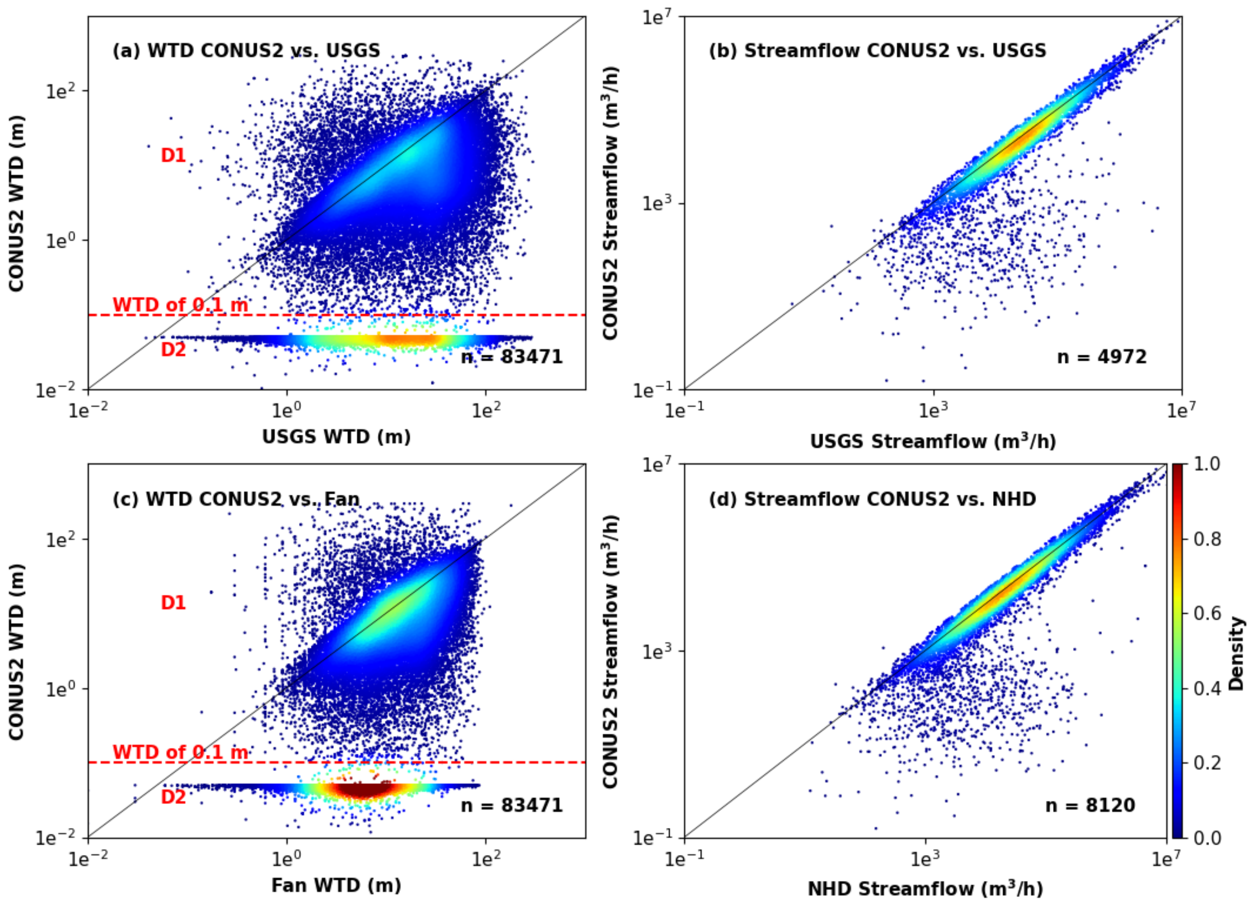

Figure 12. Scatterplots of simulated vs. observed water table depth and streamflow over the entire CONUS2 domain. (c) is plotted using random samples of the Fan dataset.

Table S1. Soil and geologic units and corresponding parameters

	Indicator	Classification	K_{sat} (m/h)	porosity [-]	Sres [-]	alpha 1/m	n [-]
Soil units	1	Sand	2.69e-1	0.38	0.14	3.55	4.16
	2	Loamy sand	4.36e-2	0.39	0.26	3.47	2.74
	3	Sandy loam	1.58e-2	0.39	0.10	2.69	2.45
	4	Silt loam	7.58e-3	0.44	0.15	0.50	2.66
	5	Silt	1.82e-2	0.49	0.10	0.66	2.66
	6	Loam	5.01e-3	0.40	0.15	1.12	2.48
	7	Sandy clay loam	5.49e-3	0.38	0.16	2.09	2.32
	8	Silty clay loam	4.68e-3	0.48	0.19	0.83	2.51
	9	Clay loam	3.39e-3	0.44	0.18	1.58	2.41
	10	Sandy clay	4.78e-3	0.39	0.30	3.31	2.20
	11	Silty clay	3.98e-3	0.48	0.23	1.62	2.32
	12	Clay	6.16e-3	0.46	0.21	1.51	2.26
Geologic units	19	Bedrock 1	5.00e-3	0.33	0.001	1.00	3.00
	20	Bedrock 2	1.00e-2	0.33	0.001	1.00	3.00
	21	f.g. sil. sedimentary	2.00e-2	0.30	0.001	1.00	3.00
	22	sil. sedimentary	3.00e-2	0.30	0.001	1.00	3.00
	23	crystalline	4.00e-2	0.10	0.001	1.00	3.00
	24	f.g. unconsolidated	5.00e-2	0.30	0.001	1.00	3.00
	25	unconsolidated	6.00e-2	0.30	0.001	1.00	3.00
	26	c.g. sil. sedimentary	8.00e-2	0.30	0.001	1.00	3.00
	27	carbonate	1.00e-1	0.10	0.001	1.00	3.00
	28	c.g. unconsolidated	2.00e-1	0.30	0.001	1.00	3.00

Table S2. RSR of logarithm transformed streamflow and WTD

Domain	Flow NHD		Flow USGS		WTD Fan		WTD USGS	
	CONUS1	CONUS2	CONUS1	CONUS2	CONUS1 (>0.4 m)	CONUS2 (>0.1 m)	CONUS1 (>0.4 m)	CONUS2 (>0.1 m)
All	1.11	0.77	1.25	0.89	1.68	1.33	1.58	1.36
2	1.92	0.20	1.11	0.17	2.17	1.32	2.10	1.16
3	1.05	0.32	1.03	0.48	3.47	1.35	5.12	2.43
4	1.60	0.37	1.37	0.57	1.94	1.67	1.99	1.59
5	0.94	0.21	1.25	0.47	2.51	0.89	3.06	0.85
6	0.92	0.18	1.39	0.52	2.53	1.70	3.06	2.48
7	0.85	0.32	0.88	0.42	2.29	1.86	1.90	1.75
8	1.04	0.13	1.40	0.70	4.17	1.93	2.63	1.28
9	2.32	1.82	2.53	2.24	1.81	1.30	1.87	1.65
10	1.21	1.00	1.34	1.11	1.32	1.18	1.39	1.29
11	1.41	1.13	1.52	1.16	1.75	1.33	1.51	1.31
12	/	3.29	0.46	1.82	4.17	3.82	2.38	1.88
13	1.74	1.82	1.93	2.37	0.89	1.10	1.79	1.60
14	1.12	0.65	1.39	0.77	0.81	1.12	0.93	1.31
15	1.12	1.41	1.21	1.38	1.26	1.35	1.78	1.68
16	1.62	1.15	1.83	1.33	1.20	1.27	1.43	1.39
17	1.15	0.68	1.43	0.85	1.64	1.47	1.45	1.27
18	2.67	4.48	1.39	1.68	1.28	1.32	1.40	1.50

Note: Original units of streamflow and WTD are m^3/h and m, respectively. The missing value is due to only one gauge in that basin in the comparison domain.

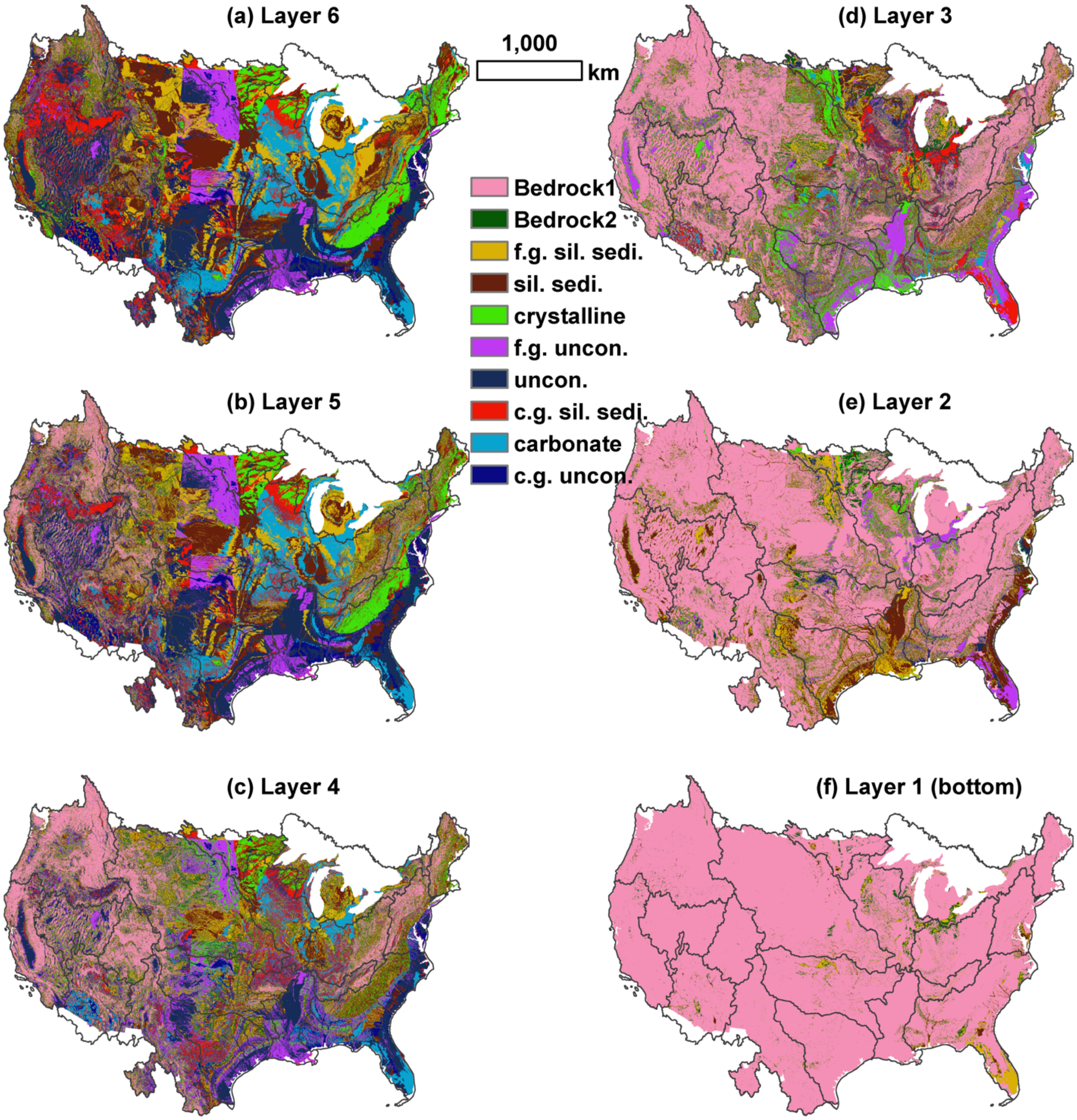

Figure S1. Geologic units of deep six layers.